Investigation and Characterization of Iron Powders for Zero-Valent Iron (Fe^0) in Synchrotron Radiations

Htay Aung Pyae, Win Win Aye, Chatpet Yossapol

Abstract*: *This study employs four differential synchrotron radiation techniques to characterize the composition of underlying Zero Valent Iron (ZVI) source in three readily commercially available iron particles (code name - M100, R12, and Scrap Iron) and highlights the importance of engaging multiple investigation methods in sourcing ZVI. With ZVI or Fe0 having reducing properties to convert harmful chemicals to harmless substances found, its widespread functional application in the environmental remediation purposes is on the rise. Consequently, attempts were being made in choosing iron powders as ZVI source in interdisciplinary researches for exploring catalytic chemical reactions of ZVI. XAS-XANES and XPS spectra revealed scrap iron could not be regarded as hopeful ZVI sources since its edges and occurrences were detected entirely in contrast against standard iron foil having noticeable valency zero, and rather resembling to iron oxides. M100 and R12 were found consisting more percentage of zero valence properties than iron foil. Homogeneity and phase identification were further investigated by mean of XRD, and discovered R12 and M100 were comparable to reference iron standards. In addition, μ-XRF uncovered possible cross contaminants existed in the samples. Finally, SEM analysis disclosed distinctive metallic morphology, formation and texture of selected iron particles. This study resolved the controversial assumption that all iron source consist of credible ZVI source for its catalytic reaction to take place. And contradictory iron oxides reactions could be highly possible on conditions when irons are not taken comparative characterization methods prior to source ZVI for requisite purpose.

Keywords*: *SEM, μ-XRF, XAS, XPS, XRD, ZVI.

I. INTRODUCTION

Among major abundant mineral reserves on earth, iron embodied about 5 percent, the fourth abundant most element on earth crust [1]. Being indispensable and cheap metal to modern world, iron plays in crucial role of human society representing 90% of all metal refined today. Application of iron in construction, manufacturing, automobile industry is because of its appealing physical properties in strength, toughness and versatility as a result of its phase, density, melting, and specific capacity [2]. With the development physical chemistry in recent decades, like other metal element, iron has been subjecting for catalytic agents for chemical reaction [3].

Manuscript published on 28 February 2019.
***** Correspondence Author (s)
Htay Aung Pyae*, Faculty of Environmental Engineering, Suranaree University of Technology, Nakhon Ratchasima, Thailand.
Win Win Aye, Department of Physics, University of Mandalay, Mandalay, Myanmar.
Chapet Yossapol, Faculty of Environmental Engineering, Suranaree University of Technology, Nakhon Ratchasima, Thailand.

Synthesised in laboratory, scientists discovered iron possesses reducing properties (oxidizing agent) as catalyst. Iron in compounds occurs in numerous oxidation states (-2 to +6), among which +2 and +3 are more prevalence in iron oxides when exposed to oxygen [4]. Being transitional element and thus highly reactive, the surface of iron particle tends to mostly reduce electron from another atom rather than reducing itself [4][5]. Earliest application of iron as chemical catalyst dated back to Habar-Bosch Process for ammonia manufacturing from nitrogen and hydrogen by iron complex in which iron speeds up the reaction at higher rate under lower temperature [6][7][8]. Fischer–Tropsch (F-T) synthesis evolved as another game changing application of iron in converting carbon-based syngas into liquid hydrocarbon [9][10][11]. By mean of catalyst irons in F-T synthesis, the higher waste-gas shift activity was proved realistic and more suitable for hydrogen and carbon monoxide exchanged was achieved [10]. Since then, iron's reactive properties became the focal point in the realm of physical chemistry and material science inspiring researchers to the potentials of iron powders as chemical addictive. While commercial grade of different iron powders are readily available in the market, iron particles could also be synthesized by dedicated chemical reactions in the laboratory scale.

The discovery of Zero-Valent Iron's (ZVI, Fe^0) properties as reducing agent to convert oxidizable substance opens new focal research to iron as catalyst for material science and applied chemistry. Though controversial, since then, the application of ZVI in environmental remediation like contaminated land and groundwater treatment as reductant or sorbent has become research attention nowadays [12] [13] [14]. In general, metallic pure iron powder, also refers to ZVI (Fe^0), oxidizes toxic and solubilize toxic substances into less harmless, stable, insoluble compounds. ZVI's active reducing properties degrades highly toxic organic contaminant and inorganic compounds under natural environment, ending itself into Fe^{2+} to Fe^{3+} [15][16][17]. The background kinetic being iron converts toxic heavy metals of different oxidation states by direct electron transfer [18]. The transformation process takes place through the adsorption or redox mechanism of its metallic oxidation state into less harmful stages [18][19]. The application of ZVI in environmental remediation measures can be classified into (1) stoichiometric ZVI reaction pertinent to dedicated pollutants as Permeable Reactive Barrier (PRB) in contaminated land or groundwater, and (2) electron transfer properties in conjunction with

aqueous compounds for redox capabilities [20][21][22]. In recent years, there has been considerable renew interests to application of ZVI in enhancing bio-methane. Researchers proves ZVI could stimulate methanogenic activities through chemically or biologically [23][24]. In particular, hypothesizing aforementioned properties of ZVI, their application into anaerobic bioreactors could accelerate microbial symbiosis among diverse fermentation bacteria and methane forming, archaea [25][26]. ZVI has been proved enhancing methane production by means of its oxidation/reduction potential to intermediary products evolved during anaerobic digestion [27]. ZVI was also proved having buffer capacity to regulate pH as a result of hydrogen gas liberated in the course of biogas processes, and consequently produce more methane [28][29]. The development of advanced electromagnetic and radiographic technologies enable research in material science with new scientific breakthroughs like never before. Apparently, with the help of spectroscopy, the properties of matter could be investigated more thoroughly in understanding to the range of materials with their electronic properties and structural heterogeneity. However, each electromagnetic radiation technique has specific function and capability to detect structural configurations and constituents. Despite adopting X-ray spectrums for materials' surface analysis, while X-ray photoelectron spectroscopy (XPS) assists in investigating a broad range of elements in their quantitative and chemical states information of the material being examined, X-ray Absorption Spectroscopy (XAS) could comprehensively detect individual element's metal oxidation states, site symmetry, coordination number, covalency, etc. Similarly, in micro-beam energy dispersive X-ray fluorescence (µ-XRF), it is designed to determine elemental composition and chemistry of material, whereas X-ray Diffraction (XRD) is applied for inspecting characterization, identification and quantitative study of material. Thanks to these techniques, researchers could speculate the properties of the substances. However, each process provides with their respective unique implications with pros and cons. Therefore, it is imperative to use multiple techniques to validate the surface composition and oxidation prior to application. Concerning ZVI application, literature reveals that researchers opted either commercially available iron powders or discarded iron scraps which were considered genuine ZVI or synthesis of ZVI in the laboratory [30][31]. Nevertheless, while pure ZVI could be synthesized, the drawback being low yield and insignificant for sizable application, commercial ZVI product needs extraordinary measures to avoid self-oxidation [32]. Especially, when ZVI is to be applied on the condition where ZVI is strictly limiting factor to achieve ideal chemical reactions. In the comparative investigation among commercially grade ZVI nanoparticles (cNZVI), iron fillings (bulk iron powder, ZVI) and synthesized ZVI (sNZVI) with no spectroscopy investigation, despite all ZVI source could improve biogas yield, cNZVI resulted best outcomes [29]. There were complex results of NZVI application, this is due to the fact that toxicity of reduced Fe species and disturbance of electron transfers [33]. In other studies, with no surface investigation by X-Ray spectrum, when three different types of ZVI (iron power, clean scrap and rusty scrap) were added to methane production from waste active sludge (WAS), iron powder performed inferior than the latter sources [26][34]. Without specifying characteristic of ZVI, iron powders addition added methane yield up to 43% [35]. In contrary, in a study of ZVI's effect on methane production, the researcher used non-rusty scrap and rusty scrap iron were investigated in anaerobic reactor, while ZVI enhanced 1.27 times of methane, scrap irons resulted better methane yields at 2.45 to 2.7 times [36]. The potential application of ZVI in scrap iron, again proved promoting methane formation when ZVI source was investigated under Energy Dispersive X-ray (EDX) [36]. However, with XRD investigation to two different commercial grade microscale ZVI powder for biogas studies, methane production could be increased up to 40% [37]. The discrepancy behind these controversial effects of ZVI being, the selection of ZVI source and ZVI verification technique. Though pure ZVI is consistent to its characteristic and properties. Therefore, it is important to use differential methods in investigation ZVI. The study aims at investigating ZVI sources prior to application in anaerobic digestion to prove whether selected ZVIs be pertaining reliable zero valency and their relative composition to ensure high bio-methane production capability, oxidation-reduction potential, and acid buffer properties. In this work, 3 different ZVIs were chosen and they were subjected to 4 differential X-Ray radiation methods in Synchrotron and one electron microscopy for characterization. The importance of comparative investigation methods in verifying ZVI has been stressed by means of individual assessment and their limitation. Finally, the study intends to highlight the importance of investigation methods in choosing ZVI application for ensuring ideal chemical reaction.

II. Experimental Procedure

A. Materials and Preparation of Iron Particles

The Zero Valent Iron (ZVI) investigation for this study was applied to two commercially available iron powder, M 100 and R12 of Swedish based metal powders manufacturer Höganäs AB Inc., and discarded scarp iron from mechanical workshop of Suranaree University of Technology. Properties of selected ZVI sources are summarized in the table (1). Prior to comparative X-ray investigations, while the surface rust of scrap iron was eliminated by octane immersed for 24 hours, rinsed thoroughly in DI water, , then dried under sunlight, powder samples were subjected under heat treatment (150 ˚C) for 24 hours in oven to shed pre-oxidized layer and avoid possible further surface oxidation by ambient air and humidity. Characterization was performed at NANOTEC-SLRI, Thailand.

Table (1): Physical Properties of Selected Iron

Samples	Apparent Density (g/cm^2)	Specific Surface (BET) (m^2/kg)	Particle Sizes
M100	2.4	130	1~100 nm
R12	1.4	225	1~100 µm
Scrap Iron	1.61 ~ 2.6	265 ~ 355	2~10 mm

Published By:
Blue Eyes Intelligence Engineering
and Sciences Publication (BEIESP)

B. Surface Analyses and Techniques

(1) X-Ray Absorption Spectroscopy (XAS)

Electron activated by bending magnet in high voltage (1.0 ~ 1.2 GeV) beam, the B.L 5.2. of SUT-NANOTEC SLRI supports energy range between 1240-12100 eV with two major modes (i.e. Transmission and Florescence) [38]. The existence of the structures around subjected element could be verified either near edge (XANES) or fine structure (XAFS) which contrast being depend on the target intended to analyses. Since this study focuses metal oxidation and covalency of elemental iron, XANES mode with ion chamber approach was applied. The beamline is capable with energy resolution up to 2 x 10^{-4}/light energy. The spectra of Fe foil, pure iron, occurs at 7112 eV. Then, samples were compared against standard iron spectra of Fe^0 (Fe), Fe^{2+} (FeO), Fe^{3+} (Fe_3O_4). Strict calibration measures were followed to prevent precision errors, biases and invalidity. Samples were treated with in situ nitrogen (N_2) gas flashing arrangement lest surface oxidation incidence prior positioning into sample chamber. Instead of adhesive coloured tape, clear plastic sachet was used in sample mounting to have x-ray attenuation and absorption in check. 6 scans were attempted to reduce spectra noises and ensure consistency between each scanning. In order to retrieve scanning data, beamline edge energy thresholds were set from ~20ev before and ~150eV above the Fe edge 7110 eV. Retrieved spectra data were further presided by Demeter XAS data processing and analysis package.

(2) X-ray Photoelectron Spectroscopy (XPS)

Following the same suit, X-ray photoelectron spectroscopy (XPS) spectra for this study was conducted in SUT-NANOTEC SLRI, B.L 5.1. By the excitation of electron in relatively shallow core level by mean of Kα surface analysis system, the XPS phenomenon itself being flexible in detecting diverse material with its functional groups, chemical compositions and state of elements, while survey scan consists of numerous sharp peaks emerged across binding energy range (0~1400 eV) with respect to intensity (c/s), whereas narrow scan accentuates specific element in which it arises within the whole spectrum. Common notation exhibit in XPS are in electron orbitals (e.g. $1s_{1/2}$, $2s_{1/2}$, $2p_{1/2}$, $2p_{3/2}$, etc.), and different electron spin located across the spectrum. Argon (Ar) gas sputtering was applied to reduce surface oxidation preceding to implant on sample platter. Thorough coarse navigation was examined through optical view window for adequate XPS point analysis. During the investigation, all samples where first underwent 2 surrey scans (0~1400 eV) to identify possible clusters, after validation, 6 narrow scans dedicating to Fe related binding energy range (705~720 eV) and spin-orbit splitting of peaks (i.e. 2s, $2p_{1/2}$ and $2p_{3/2}$) was measured. Best ZVI location source was chosen by automatic optical detector. Observed Fe peaks were further substantiated against standard XPS database and analysed using PHI multiPak XPS data processing application with a combination of Gaussian and Lorentzian components.

(3) X-Ray Diffraction (XRD)

X-ray Diffraction (XRD) technique is used to investigate the size and the shape of the unit cell of any compound. Diffraction patterns gives information on size and shape of unit cell from peak positions and information on electron density inside the unit cell, namely where the atoms are located from peak intensities. It is performed by using monochromatic Cu K-α radiation (λ=1.54056 Å), operated at 40 kV and 40 mA. Iron samples are scanned from 10 °C to 70 °C in the diffraction angle, 2θ with a step-size of 0.01°. The crystallite sizes are estimated by using Debye Scherrer's equation:

$$D_{crys} = \frac{k\lambda}{\beta cos\theta} \quad (1)$$

where,

D_{crys}=crystallite size (nm),

k=Scherrer constant (about 0.89 for Fe_3O_4 and Fe_2O_3),

λ=wavelength of Cu-K-α (λ=1.54056 Å),

θ=peak angle (deg.),

β=width of the XRD peak at half height (radian).

(4) Micro Beam Energy Dispersive X-ray Florescence (μ-XRF)

Energy dispersive micro-XRF technique is used to analysis the qualitative and quantitative composition of solid or liquid samples. It can be used to measure virtually every element from K to U in the periodic table in concentrations ranging from a few ppm to nearly 100 percent. Measurement of wavelength of the X-ray photons emitted by the sample element allows the identification of the elements present. It can permit to obtain images with element distributions on the surface of the iron samples. Powder samples are pressed into pellet (1 cm diameter) by applying pressure of 5 ton for 5 minutes using a hydraulic press. The analysed element is counted in the absorption K edge energy range of 0-15 keV in order to calibrate the energy scale. The measured spectra are fitted using fit line profiles for powder and scrap samples. To get the reliable data, the instrument is calibrated using the expected elemental concentrations from the standards vs. the calculated elemental concentration. The best fit of standards on the regression line indicates that the analysed concentrations are at or near the given concentrations.

(5) Scanning Electron Microscopy (SEM)

The surface morphology and microstructural properties of iron samples are observed by using scanning electron microscopy (SEM). The average grain size of M-100, R-12 and scrap samples are examined from the observed SEM images. It can create the maps of element distribution on the surface of samples. The device uses the electron beam to produce a magnified image of iron sample. In the device, the electron gun produces a high intensity electron beam, which passes through a series of electromagnetic lenses to be focused and scanned across the sample. The incident electron beam causes secondary electrons to be emitted from the iron sample. Then the image is reconstructed from the signals backscattered from the surface of the sample and magnified on the screen. The resolution of the SEM can approach a few nanometre (nm) and it can operate at magnifications that are easily adjusted from about 10X-300, 000X.

Published By:
Blue Eyes Intelligence Engineering
and Sciences Publication (BEIESP)

III. RESULTS AND DISCUSSION

A. X-Ray Absorption Spectroscopy (XAS) Analysis

Since XAS comprises the combination of XANES (X-ray Absorption Near Edge Structure) and EXAFS (Extended X-ray Absorption Fine Structure), while XANES (pre-edge of the spectra) infers for metal oxidation and co-valancies, whereas EXAFS (post-edge) is associated with ligands, bond angle etc. Fe XANES spectra in figure (1) reveals respective spectrum of 7 comparative irons in this study. M100, R12 and Scrap Iron were ZVI hypothesized samples, and they were evaluated against standard Fe (Fe Foil), FeO, Fe_2O_3, Fe_3O_4 having oxidation states 0, +2, +3, and +2/+3 respectively. The elemental Iron (Fe) having valency zero which the relative energy occurs at 7112 eV was the principal sample against which the concerned samples (M100, R12 and Scrap Iron) were differentiated whether owing their zero valent properties. The remaining iron oxides testified being reference the condition of different iron oxides' oxidation states and spectra patterns. The XAS results (figure: 1a) indicates that the edge of M100 and R12 arose noticeably from left to the standardized iron foil (Fe) giving evidence that the samples (M100 and R12) are consistent proof of being in zero oxidation state. In contrast, the spectra of scrap iron which occurred more isolated and shifting sparsely right to standardized iron foil (Fe) and far secluded to M100 and R12. Since the edge of Scrap Iron emerged between standard iron elemental (Fe) and Iron II oxide (FeO), it is the evidence that scrap iron's metal oxidation state (valency) is distinct to those of M 100 and R12. This is due to the fact that scrap iron which is the discarded iron fragments derived from cast, wrought and rolled iron bar or plate from machinery workshop which intrinsically had been under prolong exposure to air and contain other metal from manufacturing processes. Consequently, its surface environment was entirely oxidized. In contrast, among M100 and R12 which are genuinely specified as elemental iron powder, the spectra of R12 was discovered closer to standard Fe spectra, meaning R12 iron powder is highly in consistence with higher ZVI source. The pre-edge and edge spectra stacked plot (figure:1b) provide further confirmation that while the characteristic of elemental irons (i.e. Fe (Foil), M100, and R12) conformed to identical approach at 7112 eV, iron oxides (i.e. FeO, Fe_2O_3, and Fe_3O_4) were observed vicinity to 7120 eV respectively. And, among which Scrap Iron's appeared between 7112 eV and 7120 eV. However, XANES in XAS method in this stage could not further validate quantitatively composition of metal elements.

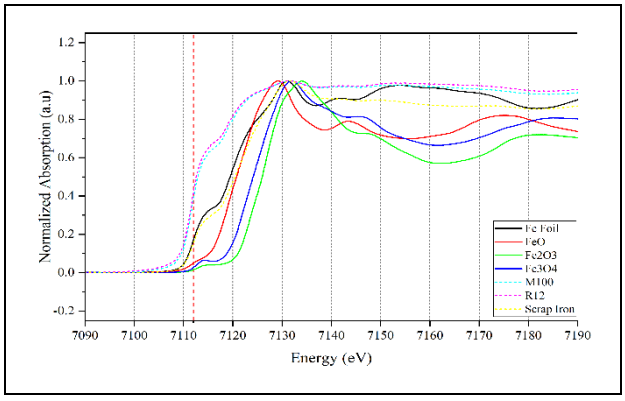

Figure 1-(a) Normalized Pre-edge and Edge

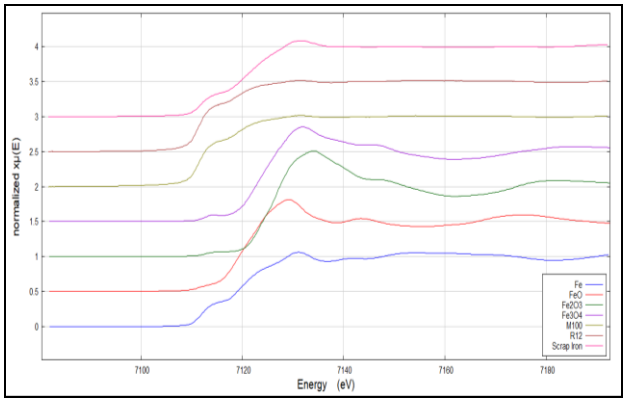

Figure 1-(b) Stacked normalized pre-edge and edge

Figure (1): XANES Spectra of Different Iron Sources

The localized spatial edges' discrepancies within Fe spectra and those of R12, M100 and Scrap iron could possibly have triggered by their distinct phases (texture, size, density, and BET) and morphology of the samples. While the standardized Fe spectra was obtained from elemental iron foil, M100 and R12 spectrums were of Micro- and Nano-particles. Nevertheless, with spectra shift in obvious eccentricity to elemental iron (Fe foil) and the peaks conformation below known oxidation state, the relative oxidation states of M100, R12 and Scrap Iron could be enumerated by contradiction to valency states of Fe, FeO, Fe_2O_3, and Fe_3O_4. By Gaussian curve fitting to all energy peaks and linear regression to x-ray absorption, the peaks of all hypothesized samples progressed below known iron oxides (Fe II, FeI II, and Fe II/III) spectrum; this ascertains that all three selected samples, with the exception of scrap iron having inferior to Fe foil in term of valency 0, M100 approached proximity to zero valence oxidation state, then followed by R12. This further substantiates that M100 and R12 hold highest zero valent credibility. Since the target samples were elemental iron (Fe) participating single iron element and with exclusion and comparison among different compounds, k,R,q space driven by EXFAS analysis and extended spectra constituency was ignored. Other potential metal impurities were further inspected by other differential methods.

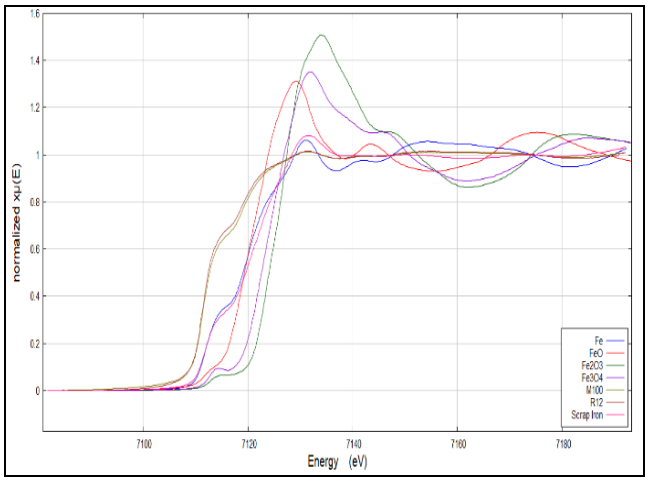

Figure 2-(a) Irons XANES peak fitting in energy excitation

Published By:
Blue Eyes Intelligence Engineering and Sciences Publication (BEIESP)

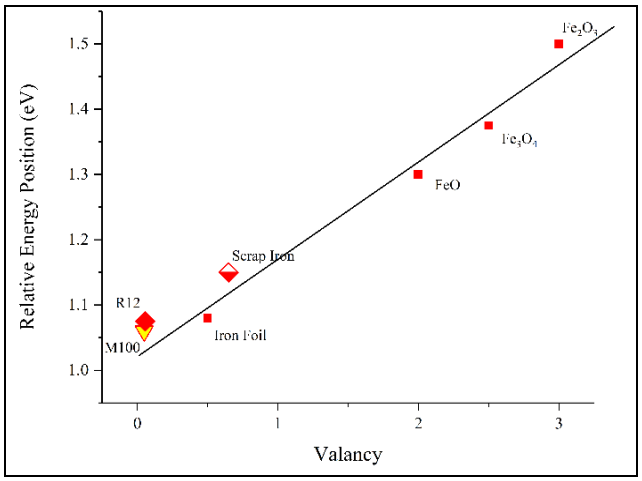

Figure2-(b) Relative Valency of Irons

Figure 2: Spatial Peak formation during energy excitation

B. X-ray Photoelectron Spectroscopy (XPS) Analysis

The advantages of XPS over XAS being capability in survey scanning (0~1400 eV) in detecting multiple atomic species and their relative quantitative concentration in the sample described in a single spectrum. Vice versa, this is also major drawback of incapability to identify specific diverse oxidation states of the metals in XPS. Therefore, separate narrow scanning for which configured binding energy range is obligatory requisite in characterizing individual elements. XPS Survey Scanning in figure (3) reveals that satellite sharp peaks were discovered in all three samples (M100, R12, Scrap Iron) representing the existence of Carbon (C), Oxygen (O) and iron (Fe) across different orbital edge. Apparent atomic Carbon and Oxygen were identified in s-shell at binding energy 285 ± 5 eV, 530 ± 5 eV, and 706 530 ± respectively.

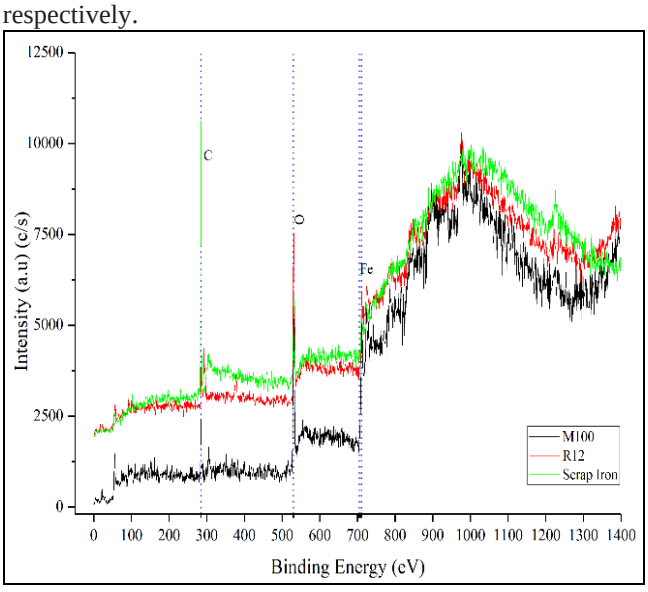

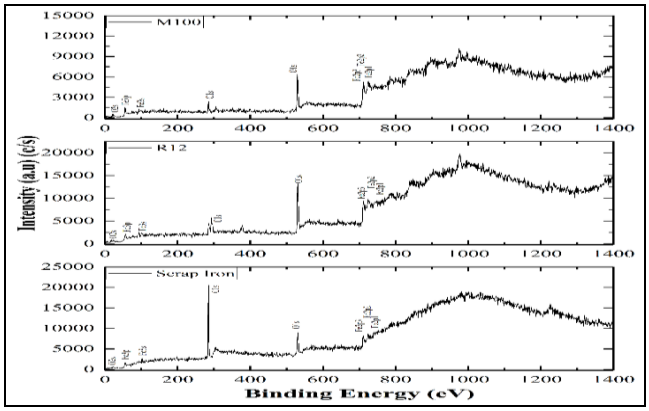

Figure (3): XPS Survey Scanning Spectrum of Irons

Numerical results generated from synchrotron light indicated that R12 had highest atomic Fe concentration with minimum atomic oxygen (Table 2). Therefore, sample R12 could be considered to have highest iron (Fe) source. This result is being controversial to those of XAS in which M100 was previously proved convincing zero valent iron source. However, the justification being while XAS focuses oxidation states of elements, XPS, on the other hand, emphasizes quantitative composition of Iron in both element and compounds by function of sharp peaks establishment. Therefore, the XPS spectra reveals different elements along wider energy range by means of peaks developed at respective energy. Followed by M100 after R12's highest iron (Fe) composition, and finally scrap iron turned out resulting lowest atomic iron and highest carbon and oxygen to its counterparts since generic scrap iron derived from smelting chains consisting higher carbon because of commercial grades and fabrication processes. Particle size and texture of the samples could also be the factor for these differences. Since the XPS surface technique analyse 2~5 nm probing depth of the sample surface, which is extremely shallow depth, with this, instantaneous oxidations could take place when subjected to local environment exposure and the rate varies as increased in particle sizes, apparent density, and relative humidity. Therefore, it is advisable other corresponding methods in validating and characterizing core-shell structure and composition. Unlike XAS, in which hypothesized samples were compared against other standardized specimen (i.e. Fe Foil, FeO, Fe_2O_3, and Fe_3O_4), in XPS investigation samples were evaluated alongside with XPS database [39].

Table (2): Atomic Concentration of Irons

Samples	Atomic Concentration (%)			
	Fe	**O**	**C**	**Others**
M100	93.01	4.85	0.66	0.48
R12	96.86	1.26	0.92	0.96
Scrap Iron	73.22	17.51	6.36	2.91

Narrow scanning in accordance to associated binding energy for focused element opens another measure in characterizing iron and its compounds. Theoretically, the peak of Zero Valent Iron (ZVI) in photoelectron spectra analysis could not be pinpointed on the generic iron spectrum since ZVI peak being tiny arc and barely unnoticeable unless samples are Ar^+ sputtered.

Published By:
Blue Eyes Intelligence Engineering
and Sciences Publication (BEIESP)

Based on the XPS narrow scanning with Argon (Ar^+) sputtering in this the study, overall Fe oxide peaks were easily distinguishable and significantly shifting at higher binding energy the metal iron (figure 3). While metal iron (Fe) peak develops between 706 ~ 708 eV, in which zero valent iron positions on the edge (figure 4b). Then, irons oxides (Fe_xO_x) in their particular orbital spinning orientation progresses after 710 eV in the Fe XPS spectrum. Since, oxides of iron peaks generally shift to higher energy level than metal state, from the experiment, it was discovered that Fe metal peak of M100 and R12 were found beneath that of Scrap iron and followed within reference energy boundaries (figure 4a). When spectra are compared in detailed against standard Ar+ sputtered Fe_2O_3 spectrum (figure 4b), all of the iron sample could possibly be oxidized to (Fe II and Fe III), among which M100 and Scrap Iron were found partially being oxidized because those spectra trend were found identical to Fe III and Fe III satellite zones.

Besides acquiring higher Fe atomic concentration and the trend of XPS spectrum of M100 and R12 were comparatively in parallel, this adds further supportive evidence that scrap iron has more oxidized characteristics. This implies that M100 and R 12 hold more oxidizing potentials. Even though, exact valance could not be interpreted from XPS spectrum, it can provide with possible oxidation states by reaction response when exposed to chemicals. The recognizable raise of scrap iron's spectra after the Fe peak proved that scrap iron is either partially or completely oxidized in surface layer during purifying processes, while the R12 and M100's spectrum remains in lower intensity as increased in binding energy. This is further proved by atomic concentration of each sample shown in table (2). The presence of other minute metal concentration could also trigger these variances. Hence, the characterization of ZVI for selected irons was further elucidated by with XRD and µ-XRF.

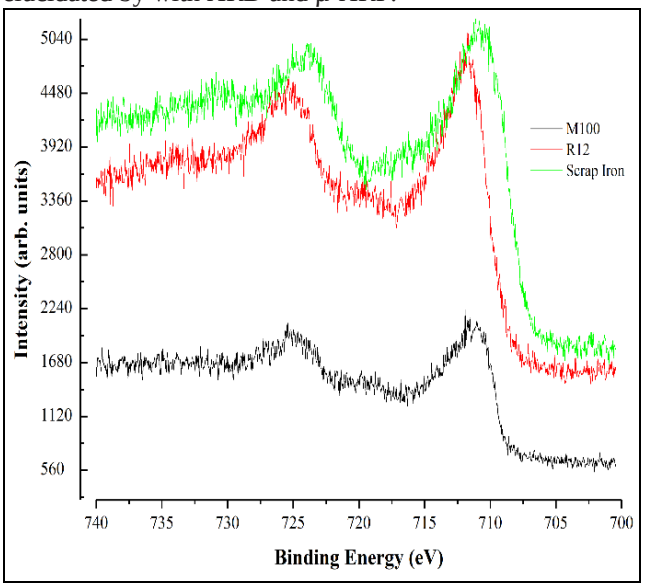

Figure 4-(a) Customized Scanning of Irons Spectra

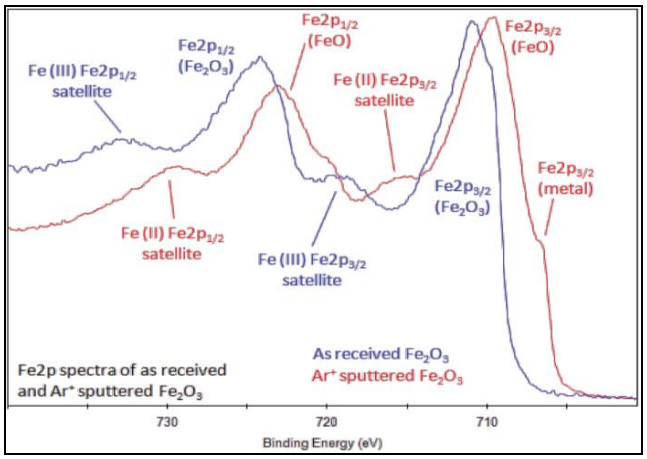

Figure 4-(b) Standard Iron Spectra orbital state. [40]

Figure (4) Narrow scanning of Irons XPS spectra and Standard Iron Spectrum

C. X-Ray Diffraction (XRD) Analysis

The XRD spectra of iron-powder and scrap were indicated as shown in figure (5). The upper side of XRD profile represents the observed profile while the lower side indicates the standard (reference) of Fe JCPDS (Joint Committee on Powder Diffraction Standards) library. Upon Compared standard data with the diffracted peaks to observed XRD pattern, the peaks were indexed. M-100 and R-12 were named for Nano and Micro size iron samples. On the iron-powder XRD patterns, there were only two identified peaks (110) and (200) at 2θ=44.61°, 65.16°. The micron size iron sample (R-12) had more intensive peaks than nanometre scale sample. Three peaks were clearly observed on the iron-scrap XRD pattern but (110) and (200) peaks at 2θ=44.68°, 64.93° were well matched with those of the standard (reference) Fe JCPDS library file. The other peak at 2θ=30° could not be identified. The diffraction line at 2θ=44.61° was the strongest in intensity among the collected M-100 and R-12 XRD lines. To calculate the crystallite size, we used the strongest diffraction line. Crystallite sizes of the M-100 and R-12 samples were obtained as 32.24 and 33.28 nm. The smallest crystallite size is iron-scrap sample and it is obtained as 16.38 nm.

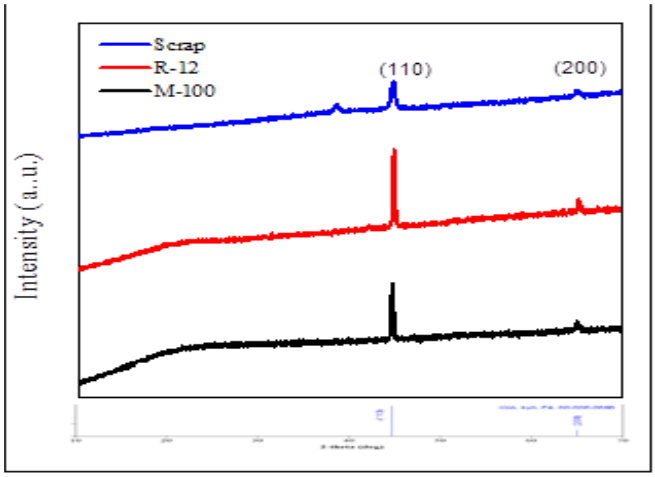

Figure (5) XRD pattern of Fe-powder and Fe-scrap

Published By:
Blue Eyes Intelligence Engineering
and Sciences Publication (BEIESP)

D. Micro Beam Energy Dispersive X-ray Florescence (µ-XRF) Analysis

Raw µ-XRF spectra were fitted using data analysis tool named PyMCA for all samples. The black line showed the experimental data. The red solid line showed the best fit of the experimental data. The green line was continuum line model where background was subtracted from the experimental data. The pattern of peaks observed in the spectrum are directly related to the elements present in the iron sample. Figure 8 (a-c) show the existence of some metals including Sc, Mn and Fe in XRF spectra. The fitted KL3 lines of Sn, Mn and Fe on each spectrum were 5900, 6490 and 7058 eV respectively. The atomic Fe concentration percentage of 67, 72 % were recorded for M-100, R-12 iron powder samples after using iron 70 % occupied material as a standard reference sample. A very high content of Mn and Fe was detected in all analysed spectra. The 0.144 and 0.148 of the full width at half maximum (FWHM) estimated on Mn and Fe peaks of spectrum and fit areas were $3.845x10^3$ and $1.118x10^6$ for R-12 and $5.8035x10^2$ and $1.048x10^6$ for M-100 at KL3 lines.

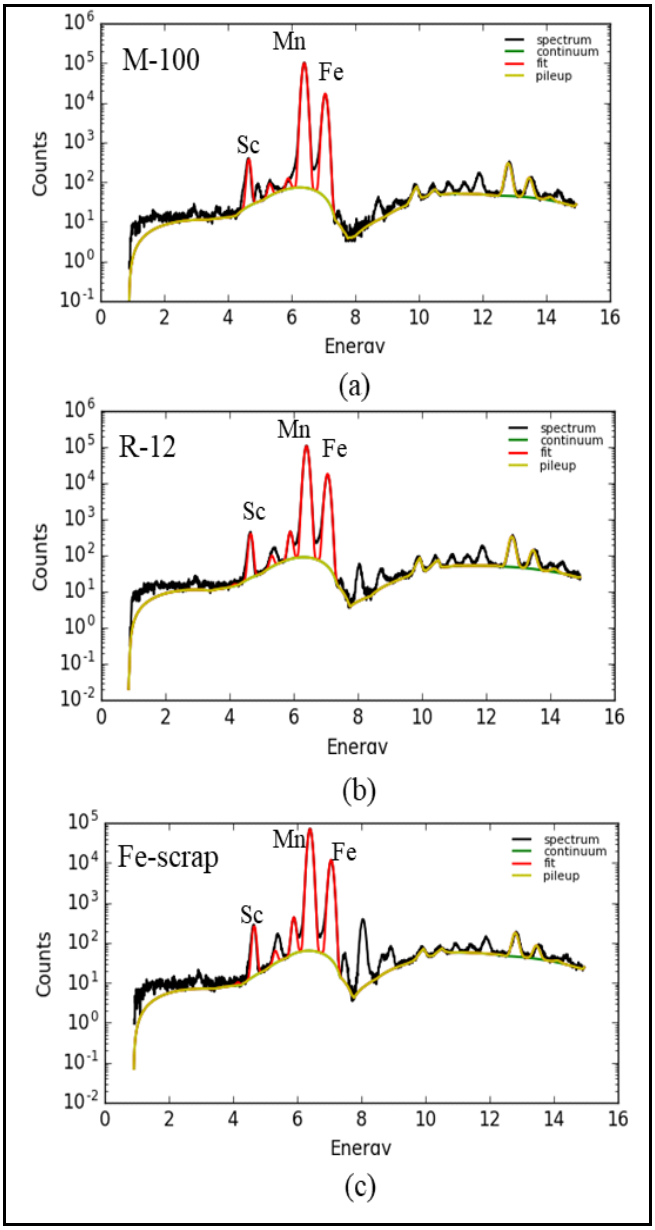

Figure (6) Fit peak results of Fe-powders (a-b) and Fe-scrap (c)

E. Scanning Electron Microscope (SEM) Analysis

The photomicrographs of iron powder and scrap samples were shown in figure 7 (a-c). Distribution and orientation of grains and compact layers in iron sample were morphologically investigated using JSM-5610 Scanning Electron Microscope (SEM) with accelerating voltage 15 kV and 850 times magnification. In all samples, same bar code system of 20 µm was used. The surface morphology of iron powders was seemed to be sponge shape and the grain sizes were apparently large in micron size R-12 samples. In Nano size M-100 sample, the agglomerated iron particles were noticeably much smaller compared to the R-12 sample. But the grain distribution was uniform. The shapes of rock layers were found in scrap sample.

Published By:
Blue Eyes Intelligence Engineering
and Sciences Publication (BEIESP)

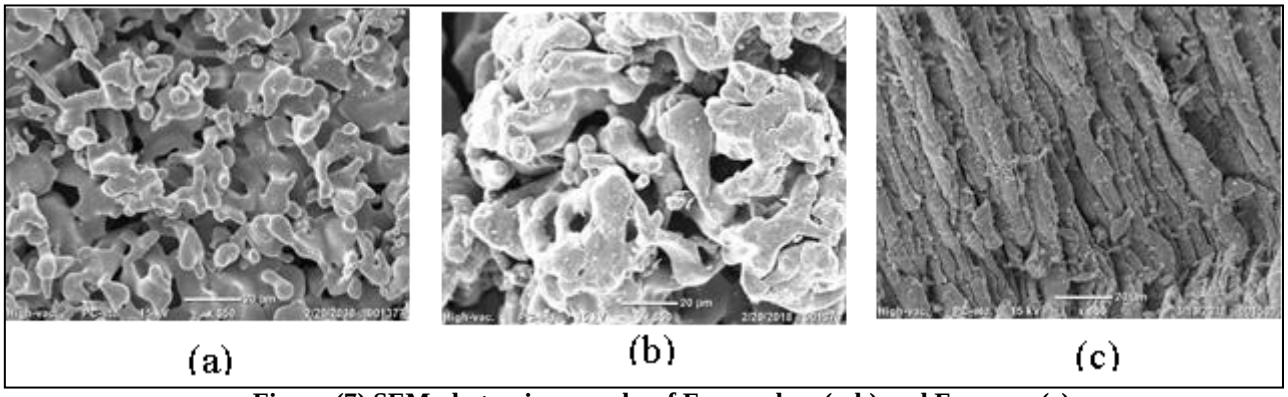

Figure (7) SEM photomicrographs of Fe-powders (a-b) and Fe-scrap (c)

The grain sizes of M-100, R-12 and scrap samples were examined from the observed SEM images. The average grain size calculated, based on image analysis was similar to the value obtained from the Scheer equation. The grain size and its distribution were presented in the form of a number-frequency histogram. As shown in figure 8 (a), the grain sizes of M-100 sample were in the range 0.5–4.5 µm. R-12 sample had minimum grain size of 1 µm and maximum grain size of 9 µm (figure. 8 (b)). The distribution curve had only one peak at 5.5 µm in size with number of grains. In figure. 8 (c), compact iron layers with different sizes in the range 0.4 – 2.0 µm were found. In R-12 sample, the presence of large grain size may be attributed to their high surface energy and high surface tension of ultrafine microparticles.

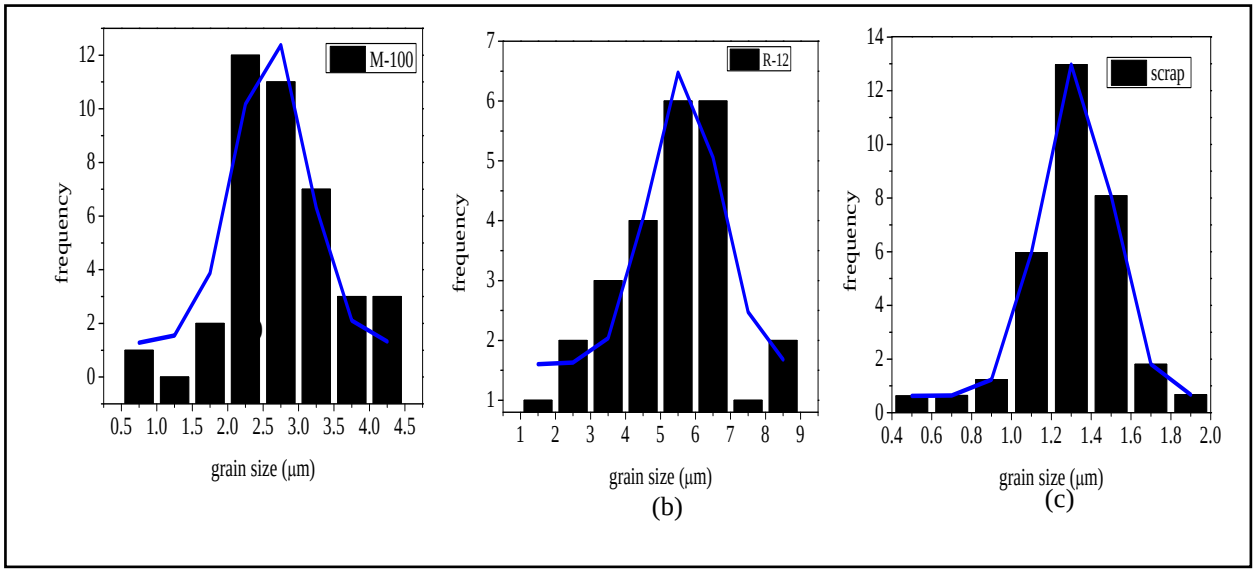

Figure (8) Size distribution histograms of Fe-powders (a-b) and Fe-scrap (c)

IV. CONCLUSION

Since widespread functional applications of zero valent iron (ZVI) as catalyst in the environmental remediation purposes, investigation and characterization is crucial lest detrimental iron reactions are eliminated, and validation is preferred if iron powder is genuinely in ultimate zero valent iron composition. In this regard, undergoing 4 differential methods to three selected iron sources (i.e. M-100, R-12 and Scrap Iron) for validating credential ZVI source. Qualitative and quantitative characterization led scrap iron was found consisting insignificant ZVI matter and apparently swayed against ZVI criteria than its counterparts (R-12 and M100). However, there could be a drawback from R12, nano-particle ZVI since it could lead to instantaneous chemical reaction than micro size grain M-100 and Scrap Iron under exposure to any liquid. It can be readily oxidized itself prior to application in intended purposes. This limitation could likely be exacerbated when nanoparticles are in contact with reactive chemical solution. Detrimental results could be envisaged due to improper handling and incorrect ZVI sourcing. Therefore, it is crucial to validate ZVI before designated reaction to be taken place. Possible paradoxical chemical outcome is also likely to be envisaged when scrap iron is undergoing application as ZVI function. By SEM investigation, the grain size distribution and particle density of selected samples was found apparently distinctive as per visual and categorial description, meanwhile, with synchrotron lights, M100 and R12 were analysed having comparable results and evidences as metallic zero valent iron, thus this two samples proved fit for enabling certain ZVI reactions for further ZVI function. However, special precaution is advisable when choosing M100 because of readily oxidizable potential (reducing or catalytic properties) by ambient exposure forming subsequent iron oxides within short period of product lifespan.

Published By:
Blue Eyes Intelligence Engineering and Sciences Publication (BEIESP)

ACKNOWLEDGEMENT

This research made possible by Suranaree University of Technology for funding, Synchrotron light Research Institute (Thailand) for beamline application, and Höganäs AB for chemicals support.

REFERENCES

1. USGS, 2008, Iron ore statistics and information, US Geological Survey Minerals Information, US Department of Interior (2008) Available at: http://minerals.usgs.gov/minerals/pubs/commodity/iron_ore/ [accessed on June 8, 2018]
2. Yellishetty, M., Ranjith, P. G., & Tharumarajah, A. (2010). Iron ore and steel production trends and material flows in the world: Is this really sustainable? Resources, conservation and recycling, 54(12), 1084-1094.
3. Pollack, S., Kaufman, R., Crosby, W. H., & Butkiewicz, J. E. (1963). Reducing agents and absorption of iron. Nature, 199(4891), 384.
4. Wilke, M., Farges, F., Petit, P. E., Brown Jr, G. E., & Martin, F. (2001). Oxidation state and coordination of Fe in minerals: An Fe K-XANES spectroscopic study. American Mineralogist, 86(5-6), 714-730.
5. Desage-El Murr, M., Fensterbank, L., & Ollivier, C. (2017). Iron and Single Electron Transfer: All is in the Ligand. Israel Journal of Chemistry, 57(12), 1160-1169.
6. Travis, T. (1993). The Haber-Bosch process: exemplar of Twentieth century chemical industry. Chemistry and Industry, (15), 581-5.
7. Kandemir, T., Schuster, M. E., Senyshyn, A., Behrens, M., & Schlögl, R. (2013). The Haber–Bosch process revisited: on the real structure and stability of "ammonia iron" under working conditions. Angewandte Chemie International Edition, 52(48), 12723-12726.
8. Kozuch, S., & Shaik, S. (2008). Kinetic-Quantum Chemical Model for Catalytic Cycles: The Haber− Bosch Process and the Effect of Reagent Concentration. The Journal of Physical Chemistry A, 112(26), 6032-6041.
9. Schulz, H. (1999). Short history and present trends of Fischer–Tropsch synthesis. Applied Catalysis A: General, 186(1-2), 3-12.
10. Dry, M. E. (2002). The fischer–tropsch process: 1950–2000. Catalysis today, 71(3-4), 227-241.
11. Van Der Laan, G. P., & Beenackers, A. A. C. M. (1999). Kinetics and selectivity of the Fischer–Tropsch synthesis: a literature review. Catalysis Reviews, 41(3-4), 255-318.
12. Khin, M. M., Nair, A. S., Babu, V. J., Murugan, R., & Ramakrishna, S. (2012). A review on nanomaterials for environmental remediation. Energy & Environmental Science, 5(8), 8075-8109.
13. Joo, S. H., & Cheng, F. (2006). Nanotechnology for environmental remediation. Springer Science & Business Media.
14. Li, X. Q., Elliott, D. W., & Zhang, W. X. (2006). Zero-valent iron nanoparticles for abatement of environmental pollutants: materials and engineering aspects. Critical reviews in solid state and materials sciences, 31(4), 111-122.
15. Zou, Y., Wang, X., Khan, A., Wang, P., Liu, Y., Alsaedi, A., ... & Wang, X. (2016). Environmental remediation and application of nanoscale zero-valent iron and its composites for the removal of heavy metal ions: a review. Environmental science & technology, 50(14), 7290-7304.
16. Noubactep, C., Caré, S., & Crane, R. (2012). Nanoscale metallic iron for environmental remediation: prospects and limitations. Water, Air, & Soil Pollution, 223(3), 1363-1382.
17. Zhang, W. X., & Elliott, D. W. (2006). Applications of iron nanoparticles for groundwater remediation. Remediation Journal, 16(2), 7-21.
18. Ansaf, K. V. K., Ambika, S., & Nambi, I. M. (2016). Performance enhancement of zero valent iron based systems using depassivators: optimization and kinetic mechanisms. Water research, 102, 436-444.
19. Boparai, H. K., Joseph, M., & O'Carroll, D. M. (2011). Kinetics and thermodynamics of cadmium ion removal by adsorption onto nano zerovalent iron particles. Journal of hazardous materials, 186(1), 458-465.
20. Fu, F., Dionysiou, D. D., & Liu, H. (2014). The use of zero-valent iron for groundwater remediation and wastewater treatment: a review. Journal of hazardous materials, 267, 194-205.
21. Cundy, A. B., Hopkinson, L., & Whitby, R. L. (2008). Use of iron-based technologies in contaminated land and groundwater remediation: A review. Science of the total environment, 400(1-3), 42-51.
22. Zou, Y., Wang, X., Khan, A., Wang, P., Liu, Y., Alsaedi, A., ... & Wang, X. (2016). Environmental remediation and application of nanoscale zero-valent iron and its composites for the removal of heavy metal ions: a review. Environmental science & technology, 50(14), 7290-7304.
23. Feng, Y., Zhang, Y., Quan, X., & Chen, S. (2014). Enhanced anaerobic digestion of waste activated sludge digestion by the addition of zero valent iron. Water research, 52, 242-250.
24. Liu, Y., Wang, Q., Zhang, Y., & Ni, B. J. (2015). Zero valent iron significantly enhances methane production from waste activated sludge by improving biochemical methane potential rather than hydrolysis rate. Scientific reports, 5, 8263.
25. Zhang, Y., Feng, Y., & Quan, X. (2015). Zero-valent iron enhanced methanogenic activity in anaerobic digestion of waste activated sludge after heat and alkali pretreatment. Waste management, 38, 297-302.
26. Liu, Y., Zhang, Y., & Ni, B. J. (2015). Zero valent iron simultaneously enhances methane production and sulfate reduction in anaerobic granular sludge reactors. Water research, 75, 292-300.
27. Shi, Z., Nurmi, J. T., & Tratnyek, P. G. (2011). Effects of nano zero-valent iron on oxidation− reduction potential. Environmental science & technology, 45(4), 1586-1592.
28. Bae, S., & Hanna, K. (2015). Reactivity of nanoscale zero-valent iron in unbuffered systems: effect of pH and Fe (II) dissolution. Environmental science & technology, 49(17), 10536-10543.
29. Carpenter, A. W., Laughton, S. N., & Wiesner, M. R. (2015). Enhanced biogas production from nanoscale zero valent iron-amended anaerobic bioreactors. Environmental engineering science, 32(8), 647-655.
30. Chekli, L., Bayatsarmadi, B., Sekine, R., Sarkar, B., Shen, A. M., Scheckel, K. G., ... & Donner, E. Analytical characterisation of nanoscale zero-valent iron: An illustrated methodological review.
31. Chang, Y. S. Synthesis of Fe-nano Particles Obtained by Borohydride Reduction with Solvent.
32. Stefaniuk, M., Oleszczuk, P., & Ok, Y. S. (2016). Review on nano zerovalent iron (nZVI): from synthesis to environmental applications. Chemical Engineering Journal, 287, 618-632.
33. Yang, Y., Guo, J., & Hu, Z. (2013). Impact of nano zero valent iron (NZVI) on methanogenic activity and population dynamics in anaerobic digestion. Water research, 47(17), 6790-6800.
34. Ibrahim, S. H., & Abdulaziz, M. (2016). The Effect of Different Zero-Valent Iron Sources on Biogas Production from Waste Sludge Anaerobic Digestion. Journal of Biotechnology Research, 2(8), 59-67.
35. Ignace, A. C., Fidèle, S., Dimon, B., Franck, Y., Lyde, T. A., Daouda, M., & Eni, A. C. Biogas Recovery from Sewage Sludge during Anaerobic Digestion Process: Effect of Iron powder on Methane yield.
36. Zhen, G., Lu, X., Li, Y. Y., Liu, Y., & Zhao, Y. (2015). Influence of zero valent scrap iron (ZVSI) supply on methane production from waste activated sludge. Chemical Engineering Journal, 263, 461-470.
37. Sreekanth, K. M., & Sahu, D. (2015). Effect of iron oxide nanoparticle in bio digestion of a portable food-waste digester. Journal of Chemical and Pharmaceutical Research, 7(9), 353-359.
38. Kidkhunthod, P. (2017). Structural studies of advanced functional materials by synchrotron-based x-ray absorption spectroscopy: BL5. 2 at SLRI, Thailand. Advances in Natural Sciences: Nanoscience and Nanotechnology, 8(3), 035007.
39. NIST, X. (2018). ray Photoelectron Spectroscopy (XPS) Database, Version 3.5. NIST X-ray Photoelectron Spectroscopy (XPS) Database, Version, 3.
40. Scientific, H. (2014). webpage on the Internet. Oxygen.[Accessed 20 April 2015]. Available from http://xpssimplified. com/elements/oxygen. php.

AUTHORS PROFILE

Htay Aung Pyae received B.Eng (Civil) from Hmawbi University, Yangaon, Myanmar, and M.Eng (Civil) from Technological University, Yangon, Myanmar. Currently, he is pursuing Ph.D degree at Suranaree University of Technology, Nakhon Ratchasima, Thailand. He has published several research journals relating to the field of environmental engineering. His contribution to academic could be find on following link:
https://www.researchgate.net/profile/Htay_Aung_Pyae

Published By:
Blue Eyes Intelligence Engineering and Sciences Publication (BEIESP)

Win Win Aye graduated with a PhD from Mandalay University, Myanmar after awarding Panacea Scholarship funded by European Commission in 2017. During this time she used Synchrotron-based spectroscopy techniques to study the surface behavior of organic aqueous solutions at the Swedish National Synchrotron Facility MAX laboratory, Lund University. She visited Dr Prayoon Songsiriritthigul's group, Synchrotron Light Research Institutes (SLRI), Suranaree University of Technology (SUT), Korat, Thailand as a Postdoctoral student (May-2017). She conducted research activities on the 'Applications of Synchrotron Radiation on Investigations of Various Materials'. In addition, she took part in supervising MSc and PhD students in Dr. Prayoon Songsiriritthigul's group. At present, she is an Assistant Lecturer at the Department of Physics, Mandalay University, Myanmar.

Chatpet Yossapol received B.Eng (Environmental Engineering) from Khon Kaen University, Thailand in 1990. He pursued M.Eng (Environmental Engineering) from Chulalongkorn University, Thailand in 1994. Then, he obtained Ph.D. in Engineering from New Jersey Institute of Technology, U.S.A in 2006. His key expertise are Environmental Impact Assessment, Pollution Control, Water and Wastewater Treatment, Solid Waste Management and other environmental interdisciplinary filed related to environmental engineering. Currently, he is acting lecturer cum deputy director for Science and Technological Equipment Center (CSTE) at Suranaree University of Technology. He publishes many publications in his career. Some of his achievements could found on https://www.researchgate.net/profile/Chatpet_Yossapol